JTTEE5 18:65–74
DOI: 10.1007/s11666-008-9243-8
1059-9630/$19.00 © ASM International

Modified Indentation Techniques to Probe Inelasticity in Ni-5%Al Coatings from Different Processes

W.B. Choi, Y. Wu, S. Sampath, and A. Gouldstone

(Submitted April 24, 2008; in revised form June 28, 2008)

In this study, two types of indentation experiments were performed on metallic (Ni-5%Al) coatings prepared by cold spray, high velocity oxy-fuel and air plasma spray. In the first type, spherical tips were used with increasing loads, and subsurface deformation was observed using a modified bonded interface technique. In the second type, cyclic loading was imposed with a sharp tip, and tip displacement was continuously recorded. Results suggest that cold spray coatings are brittle under contact loads in their as-sprayed condition, and that they exhibit a size effect that is quite different from those of the other coatings. That is to say, heterogeneities in mechanical behavior exist not as much on the single particle level as expected, but on a much larger scale of order 100 microns. This is attributed to long unbonded regions between particles, in a coating of otherwise high density. Fracture mechanics arguments support this hypothesis.

Keywords fracture, indentation, spray deposition

1. Introduction

Cold sprayed (CS) coatings are fabricated via the acceleration and impact of powder particles onto a target substrate. CS deposition does not involve the in-flight melting of particles; bonding is achieved by dissipation of kinetic energy to localized melting. For this reason, CS has advantages over other thermal spray (TS) processes in that oxidation does not occur, and >99% dense coatings are formed (Ref 1-3). In addition, quenching and thermal stresses are minimal, so coatings may be fabricated to high (2-3 mm) thickness without debonding. CS materials have been demonstrated for a wide range of metals, ceramics, and cermets (e.g., Ref 4-11), and microstructures appear dense and homogeneous in all cases, making this a potential alternative for many thick film applications.

The properties of CS materials relative to their bulk counterparts have not been fully characterized and are not predictable given process parameters as input. Further, it is not known how feedstock material properties affect coating behavior, and no general coating properties have been ascertained, for 'metals' for example. This is due to the complex nature of interparticle bonding that is still poorly understood. Models and experiments have indicated that an adiabatic shear instability exists in local regions of interparticle contact upon impact, where the high rates of plastic strain cause sufficient heating for melting, and thus bonding (Ref 12). In the models, a critical velocity (V_c) exists, below which particles will not bond, but simply land, and in some cases, rebound completely. Thus, although CS coatings may be close to fully dense, they may not be fully bonded. This has been demonstrated in a number of investigations on mechanical, thermal, and electronic properties (Ref 13, 14). Although the specific contributions to, e.g., elastic modulus, thermal conductivity, and electrical conductivity have not been separated, qualitatively CS materials are known to behave as composites (e.g., Ref 14) of bulk material and interfaces. However, a number of questions remain unanswered, in particular regarding the inelastic behavior of CS materials—information that is critical for wear and/or machining processes, as well as providing insight into the nature of interparticle bonding. Some investigations have been performed on large-scale tensile specimens of CS metals, to measure ductility and ultimate tensile strength under monotonic loading (Ref 15). These have shown that a short heat treating cycle usually improves ductility significantly, via particle work hardening recovery and presumably interparticle sintering. However, connections to tribological mechanisms that impose localized compressive loading cannot be made using these techniques.

Contact-based methods, i.e., hardness/indentation tests, are more closely correlated to the inelastic behavior observed under tribological loading. In addition to this, it could be argued that the loading mode during such tests allows greater access to (i) the progression of inelasticity and (ii) spatial heterogeneities in mechanical behavior. However, the disadvantages to indentation include the following: (a) difficulty in characterizing the subsurface deformed region, (b) 'averaging' of anisotropic or heterogeneous behavior under such compressive and multiaxial

W.B. Choi, Y. Wu, and **S. Sampath**, Center for Thermal Spray Research, Stony Brook University, Stony Brook, NY 11794-2275; and **A. Gouldstone**, Department of Mechanical and Industrial Engineering, Northeastern University, Boston, MA 02115. Contact e-mail: bubbleraft@gmail.com.

loading, and (c) lack of significant damage or material removal. Considering (c), this makes the test less sensitive to microstructural changes than, for example, a wear or scratch test. In this study, these concerns are addressed with the application of two new indent-based techniques for the characterization of a metallic CS system, Ni-5%Al. In the first one, a modified bonded-interface technique was used to image subsurface deformation under indentation testing of TS materials and ceramics (Ref 16, 17) and imaged the precise region of subsurface inelastic strain by recourse to optical microscopy and scanning white light interferometry. The optical microscopy revealed subsurface cracking, and the interferometry showed the spatial extent of inelastic strain fields, regardless of mechanism. In the second technique, low frequency (0.2 Hz) cyclic indentation and continuously monitored tip end-displacement, allowing detection of gradual or discrete inelastic events was performed. Results from CS materials were compared to those for (same feedstock) coatings deposited via air plasma spray (APS) and high velocity oxy fuel (HVOF) processes, and bulk materials, where applicable.

Note that in this paper, the term 'inelastic' is used to denote any behavior beyond an elastic limit (cracking, dislocation flow, splat sliding, compaction, etc.); the term 'plastic' would be perfectly acceptable but is often erroneously associated with dislocation flow. Thus 'inelastic' avoids confusion. Where appropriate, the mechanism of inelasticity is specified.

2. Materials and Methods

2.1 Coatings & Characterization

Ni-5%Al pre-alloyed feedstock was deposited via APS, HVOF, and CS processes, specific conditions of which are described in the literature (Ref 13). The Ni-5%Al feedstock was Metco 2008NS with mean particle diameter of 45 μm. Coatings were deposited on low-carbon steel substrates that were pre-roughened with grit blasting. APS and HVOF coatings were deposited using Sulzer Metco (SM) Plasma Technik (PT) F4 and DJ2700 spray guns (Sulzer Metco, Switzerland), respectively. APS process had particle velocity of 121 ± 19 m/s and temperature 2340 ± 126 °C and HVOF had particle velocity of 621 ± 111 m/s and temperature 1819 ± 167 °C (Ref 13). CS samples were prepared in Sandia National Laboratories, Albuquerque, NM, with an independently developed de Laval Type spray system (review Ref 18). In all three coatings, the final coating thickness was about 2 mm. Elastic modulus was 105 ± 17 GPa, 172 ± 17 GPa, and 110 ± 31 GPa for APS, HVOF, and CS, respectively (Ref 13).

2.2 Modified Bonded Interface Technique

Figure 1 shows a schematic of the modified bonded interface (MBI) technique. Samples were prepared into sandwich assemblies, which consisted of cutting samples in cross-section with a diamond wheel, and then polishing opposite faces with up to 0.5 μm Al_2O_3 suspension. Faces were then held together using cyanoacrylate glue and a mechanical press. The assembly was indented (at the interface) with a 1/8″ (3.175 mm) diameter spherical WC-Co indenter under five different loads of 50, 100, 200, 300, and 500 N (Mitutoyo AVK-C2). Indentations were at least 5 mm apart. After unloading, faces were separated and optical micrographs were taken in cross section. Note that in such a bonded interface preparation, the faces are not in perfect contact, and in fact there is a several micron separation; this separation has been shown to remain Hertzian if contact diameter $2a$ is large enough (Ref 19, 20). Nevertheless, the separation allows submicron 'bulging' to occur into the gap—and if this remains after unloading, it may be interpreted as inelastic deformation. Precise measurement of this is difficult using optical or SEM methods, so scanning white light interferometry (NewView 600, Zygo Corp. Newfield CT) was used.

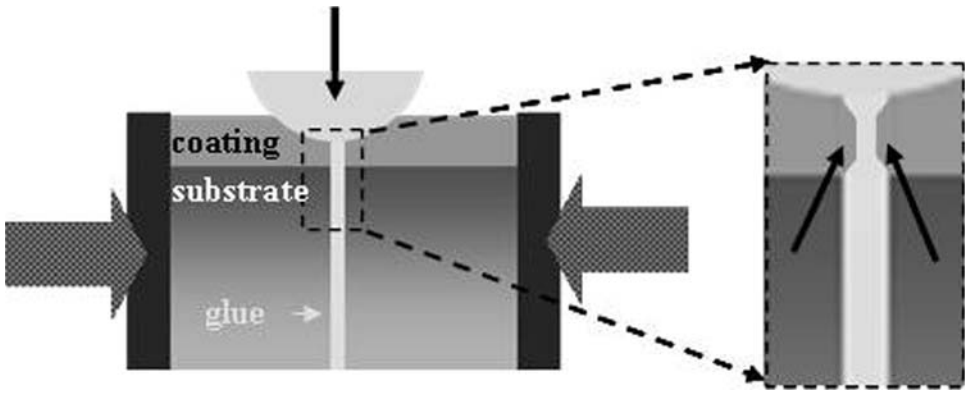

Fig. 1 Schematic of modified bonded interface technique. Coating/substrate specimen is cut, and opposing cross sections and top surface are polished. Cross sections are glued and pressed together, and spherical indentation is carried out on the seam. After indentation, the glue is dissolved and subsurface deformation may be observed (e.g., Ref 19). Poisson effects cause material to 'bulge' into the seam between faces (black arrows in right schematic); if deformation is inelastic, these bulges will persist after unloading, and can be measured under scanning white light interferometry

The depth profile of the 2-dimensional scanned cross section was modified to produce a binary image. The threshold value was set to 0.5 μm, so any region with a height greater than this was considered deformed and set to "1" in the image, and vice versa set to "0" for undeformed regions. In this way, the bright zone of an image was denoted as inelastically deformed. This technique was tested with bulk low-carbon steel specimens, and the experimentally determined inelastic zone compared very closely with FEM models (Fig. 2) (Ref 21). All coatings in this study were examined using this technique.

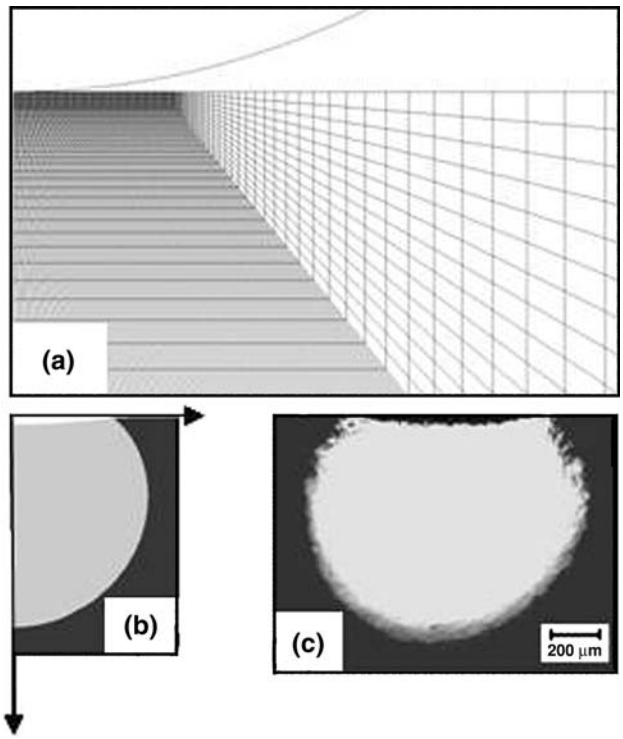

Fig. 2 (a) FEM mesh used to model spherical indentation (Ref 21); Input properties were $E = 210$ GPa, $\sigma_y = 500$ MPa. (b) Contour of accumulated inelastic strain in a cross section of material—gray area represents a value greater than zero. (c) Results of MBI experiment on low-carbon steel, showing inelastic zone with similar shape to FEM result. Both model and experiment are shown for a 1/8″ indenter tip, under 500 N load

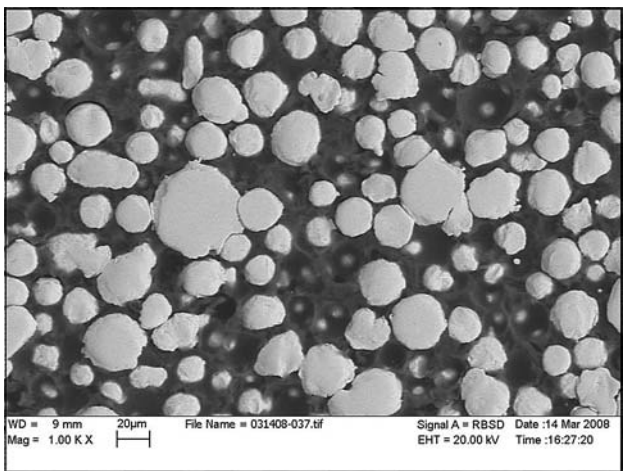

Fig. 3 SEM micrographs of the powders used in the experiments

2.3 Microdynamic Impact/Fatigue (MIF) Test

The MIF experiments have been described in detail elsewhere (Ref 22, 23), but salient points and resulting protocols are presented here. A cube corner tip (nominally sharp for our size scale) was imprinted into the tested specimen to a maximum load (either 100 mN or 500 mN) and tip displacement was recorded. After 5 s at

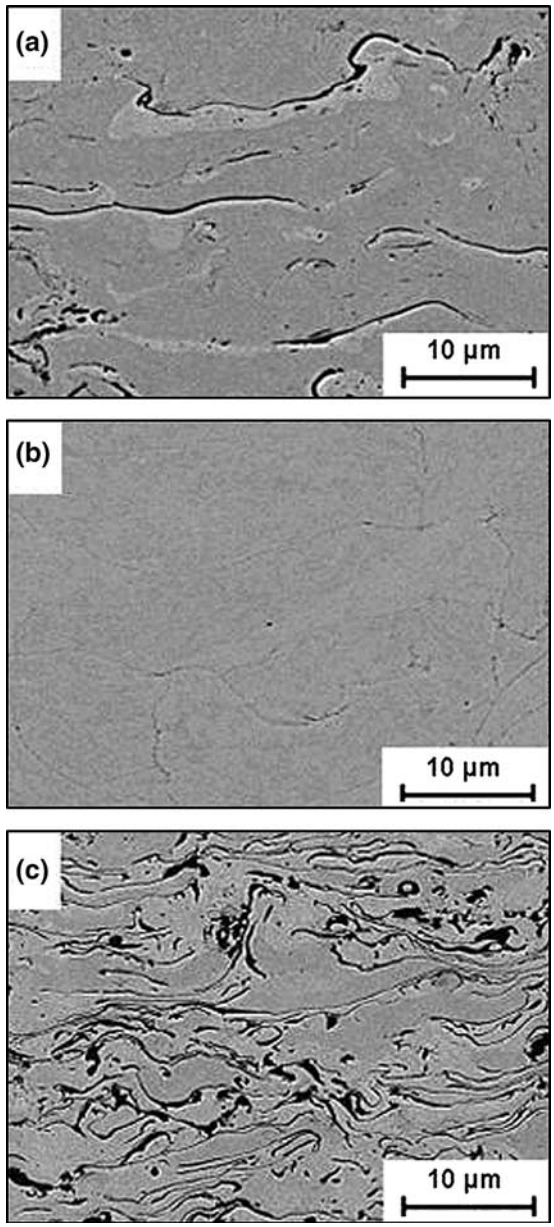

Fig. 4 Cross-sectional polished and etched SEM micrographs of coatings: (a) HVOF, (b) CS, and (c) APS

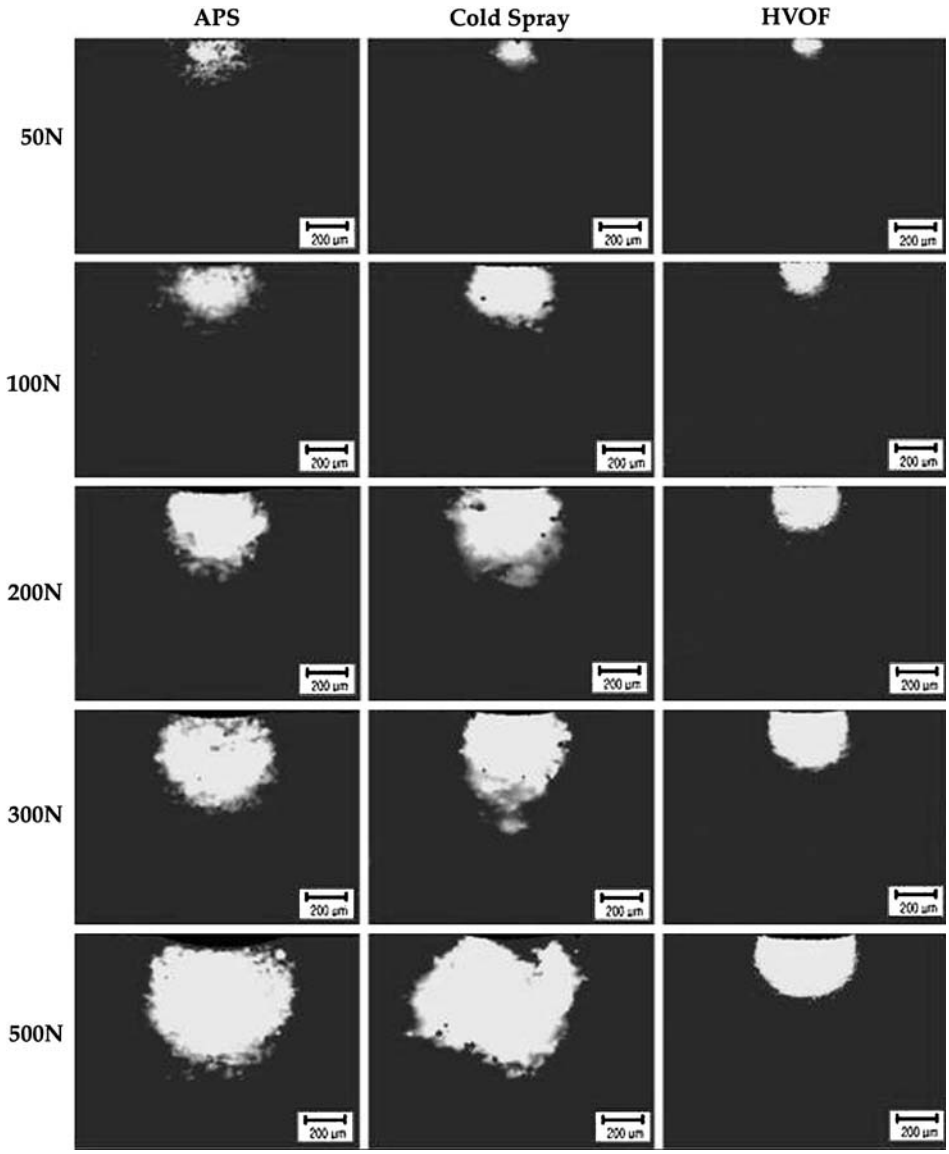

Fig. 5 Converted-to-binary images for coatings under different indentation loads. Bright regions indicate inelastic deformation. Coatings are labeled on the images

maximum load, the tip was retracted out of the specimen to a distance 40 μm above, and held for 1 s. Following this, the tip was repeatedly impacted into the specimen at a velocity of approximately 45 μm/s, to maximum load, held for 5 s, then unloaded. Cycling persisted for 1 h (approx. 300 cycles) and tip displacement was recorded at a rate of 1/s. Five tests were performed on coatings deposited by all three methods. Indentations were performed 500 microns apart, as determined by machine software.

3. Results

3.1 Microstructural Characterization

Figures 3 and 4 show SEM of powder feedstock and coating cross sections, respectively. Features are typical—HVOF (4a) shows less oxidation than APS (4c), and both display a lamellar structure. The CS (4b) appears fully dense, with little oxidation (black marks). These coatings are identical to those reported in ref (Ref 13), and full characterization appears there.

3.2 Modified Bonded Interface

Figure 5 shows the converted binary images of subsurface deformed regions for CS, APS, and HVOF materials under different loads. Contact diameter $2a$ was between 150 and 600 μm, resulting in contact pressure of 0.8 to 3 GPa. Note that the shape of the inelastic zone in APS evolves into what is expected for a bulk, homogeneous isotropic metal undergoing von Mises dislocation flow (see Fig. 2). At the lowest loads, regions of inelasticity are on splat size scale. Similar results are seen in

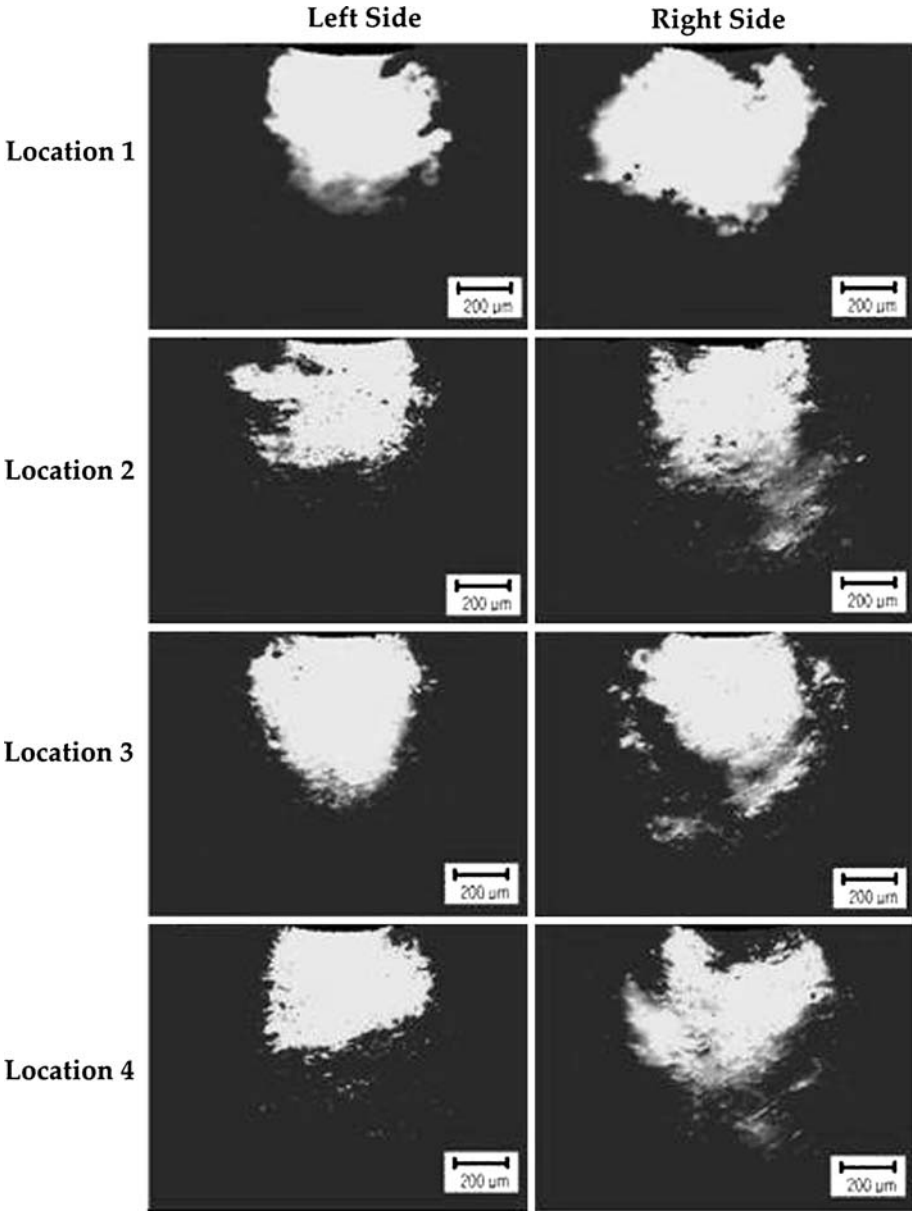

Fig. 6 Inelastic deformation in CS under 500 N loading for different cases. Note the lack of similarity between deformed regions. 'Left Side' and 'Right Side' describe both sides of the seam that was indented

HVOF, except the latter exhibits more anisotropy, in that in-plane expansion is confined. For the CS, the inelastic zone grows and is very similar to the APS results, especially at 200 and 300 N. However, at 500 N the shape is no longer symmetric, indicating local regions of inelastic deformation. To confirm this was not an effect of a tilted indenter tip, the 500 N load was repeated four times and results are shown in Fig. 6; the inelastic zones in all cases exhibit asymmetric shape, and minimal similarity with each other. Figure 7 shows optical cross-sectional images of the deformed regions, correlating to the interferometry observations. APS and HVOF coatings show high contrast, and localized, symmetric deformation near the contact region. CS coatings under the same magnification show clear fracture between particles, and the deformed region does not grow in the same manner as the other two; it shows distinct regions of cracking, away from the contact zone, as shown by arrows. In addition, the region loses symmetry at higher loads. Figure 8 shows higher magnification images of all three coatings in the contact region, displaying significant cracking in the cold spray coatings.

3.3 MIF Test

Figure 9 shows a plot of impact penetration depth vs. number of cycles for 100 and 500 mN loads on the CS materials, compared with conventional HVOF and APS

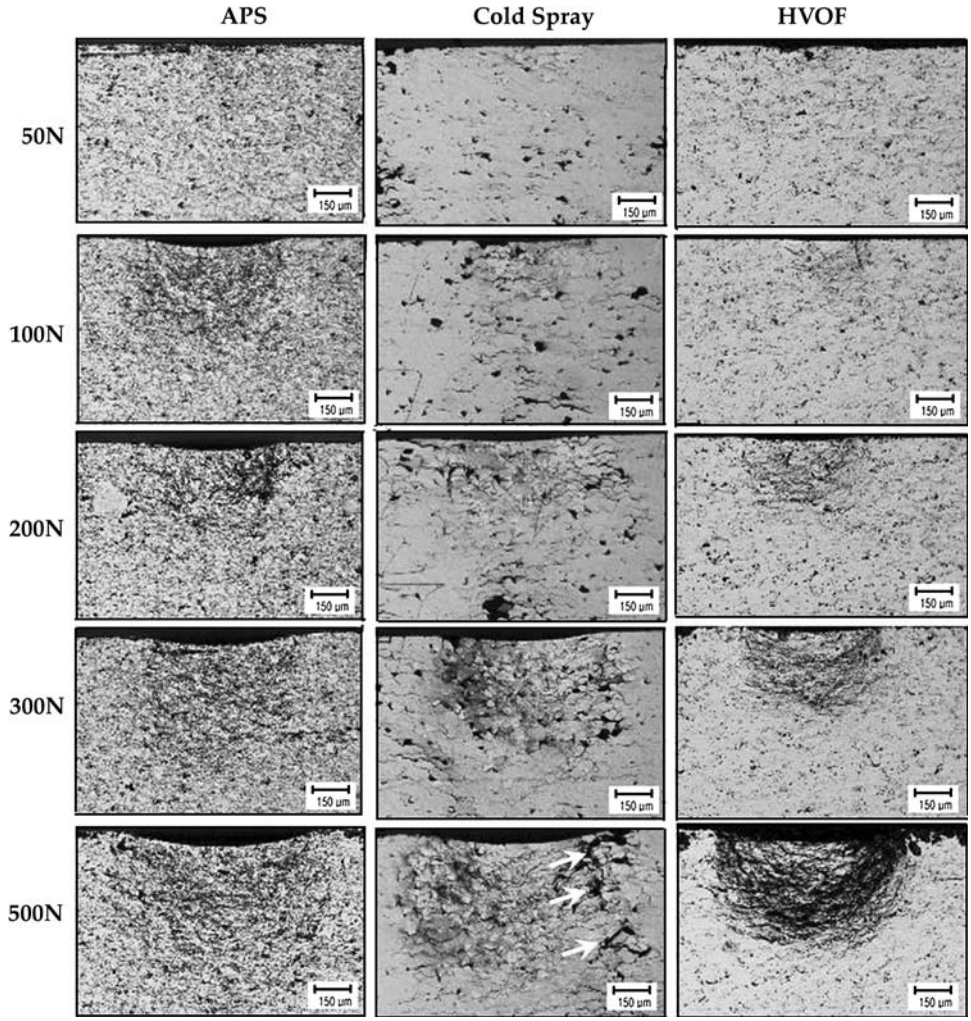

Fig. 7 Optical micrographs of coatings under different indentation loads. Note the localization of damage in APS and HVOF, as expected. CS materials exhibit cracking far away from the contact region (e.g., white arrows). Black dots are pull outs from polishing

materials. Each curve represents five independent cycles on the coatings. Figure 10 shows evolution of impact depth with the first few cycles. The following are the salient features:

(1) Within a few hundred cycles, the tip reaches a constant saturation depth under the repeated loading for all coatings. Upon reaching saturation depth, there was no sudden increase in penetration depth during the course of the impact cycles in HVOF or APS, indicating that no fast brittle event occurred that was detectable by this system.
(2) For some cases (high impact load) CS showed discontinuities, indicating fracture events.
(3) For the lower impact loads (100 mN max), the HVOF exhibited the highest resistance to deformation, and the APS exhibited the least. This was observed from the first impact event (Fig. 10) through saturation (Fig. 9). Some data spread was seen, but the overall rank remained the same.
(4) For the higher impact loads (500 mN max), the HVOF exhibited the highest resistance, but the CS showed a large spread in tip depth, both at the first impact event, and at saturation.

4. Discussion

Results from all tests indicate that the CS materials in this study (Ni-5%Al) are brittle in their as-sprayed condition. Such behavior has been observed, of course, in a number of other metallic CS systems, under tensile (Ref 15) and wear testing (Ref 24). In addition, high resolution microscopy images in the literature have confirmed high dislocation density corresponding to work hardening upon impact (Ref 25). Finally, the ductility of sprayed metals and intermetallics across a range of processes is known to be lower than that for bulk-annealed counterparts, due to the existence of defects (e.g., Ref 13). Indentation tests have been performed on Ni-5%Al

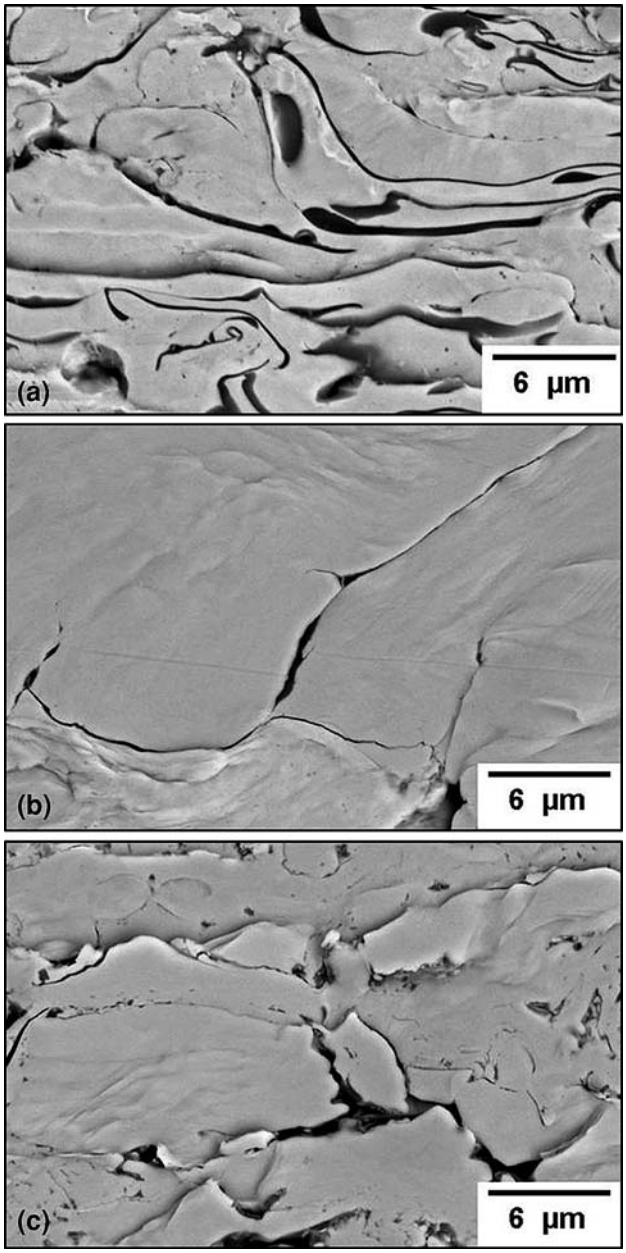

Fig. 8 Ni-5%Al cross-sectional SEM micrograph of indentation-induced subsurface damage of (a) APS, (b) Cold Spray, and (c) HVOF

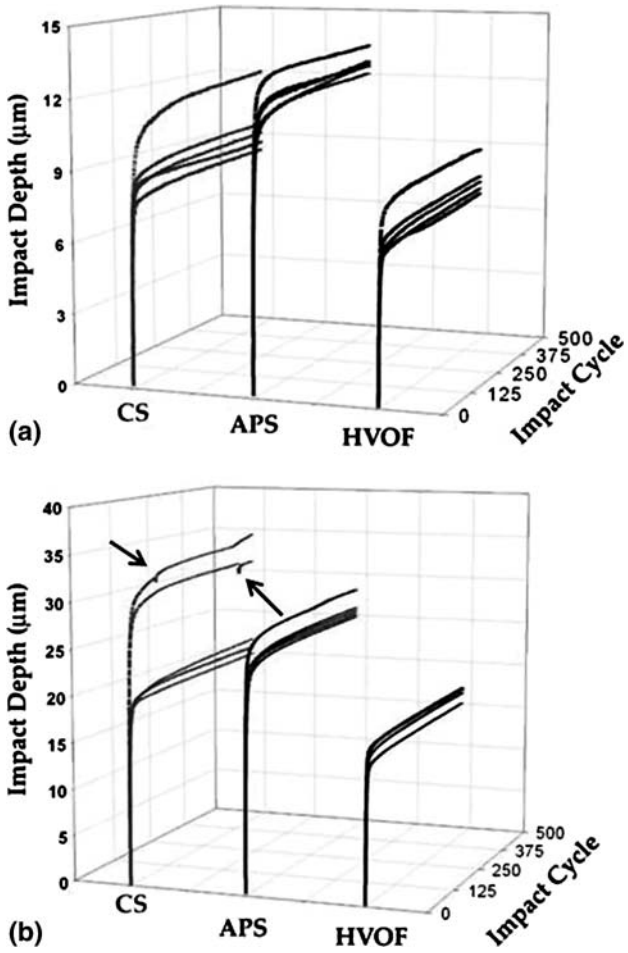

Fig. 9 Plot of impact depth versus cycle for (a) 100 mN and (b) 500 mN maximum load

coatings to produce contact stress-strain curves, and the inelastic mechanical properties of CS were found to lie between those for HVOF and APS. CS interfaces are weaker than those in HVOF, but this has not been quantified, nor the mechanisms fully explored. The former issue is due to the experimental difficulty in isolating splat interfaces for meaningful data extraction. Nevertheless the results from this study allow some further discussion of the mechanisms, presented here.

First, the CS materials in this study exhibit an unexpected size effect, that is to say, heterogeneity in mechanical behavior (i.e., local weak regions) is not apparent on the length scale of single or several splats, but more so at much larger length scales. This appears to be different from typical sprayed coating behavior, in which homogeneity emerges when more than several splats are sampled (Ref 26). These results can be rationalized by considering the differences in bonding between particles, and the intrinsic properties of the particles themselves.

APS and HVOF have similar bonding characteristics. Particles are molten when they impact, creating a metallurgical bond (a simplified statement but sufficient for this discussion). The impact of fluid on substrates with significant topography leads to interlamellar porosity. Flattening ratio in these processes is high, so no significant cracks exist that lie in the spray direction; one may approximate that the longest vertical cracks that exist would be of order splat thickness (1 micron). However, globular pores exist as a result of, e.g., fluid instabilities during spreading (e.g., review Ref 27). Splats solidify quickly, and grain size is of order 100-1000 nm, giving higher yield strength than well-annealed bulk values. In contrast, in CS, particles are solid upon impact, and if any metallurgical (diffusion-based) bonding occurs, it is due to local heating from adiabatic shear instabilities, in regions of rapid strain (Ref 12).

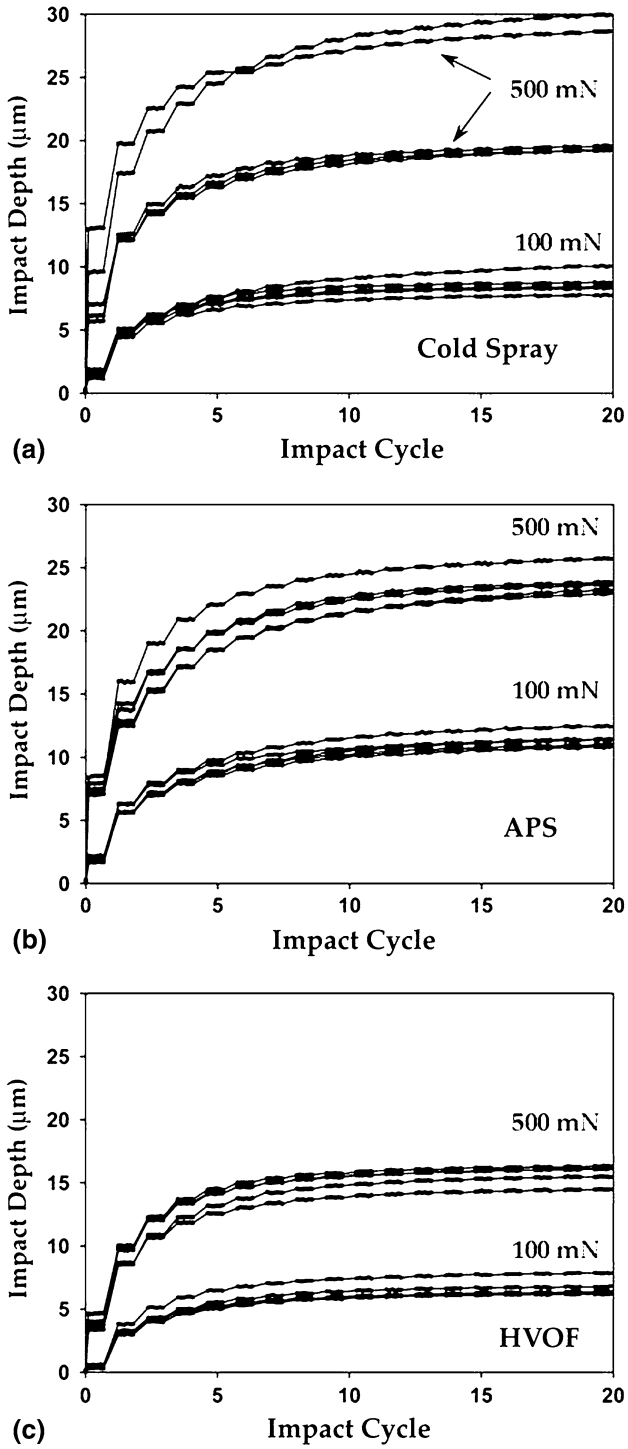

Fig. 10 Plot of impact depth versus cycle for the first few cycles

Although the existence of metallurgical bonding in CS materials is still being debated, it has been shown in models that it would occur at splat 'corners' and extend inward. The spatial extent of bonding is dependent upon modeling assumptions, and is experimentally unknown. In their well-cited models, Assadi et al. assert that critical velocities would lead to a 15-20% surface area bonding, but this has not been confirmed (Ref 12). Price et al. heat-treated Cu-Al CS materials, and inferred bonding fraction from intermetallic formation. Their values were closer to 40% surface area bonding for single particles on substrates (Ref 28). In CS, significant flattening does not occur, and impacted particle height is still of the order of initial particle size. This leaves an unbonded region between splats with length of the order of particle diameter D. (In the present study, $D \sim 45$ μm.) A similar, vertical crack length appears between particles, and this has been shown indirectly in the literature (Ref 14). Finally, another major difference is the overall density; CS coatings are typically greater than 99% dense, with few or no globular pores.

The apparently consistent mechanical response, regardless of test location on the smaller scale can be addressed by considering the high density of CS materials; indentations in different regions will contact splats, with no underlying pores. Thus, compliance and hardness will be consistent regardless of location. APS and HVOF coatings, as is known, exhibit high variation in small-load indentations due to the aforementioned pores, and this variation disappears as a larger volume is sampled.

At higher sampling volumes, it seems inelasticity is dominated by the interfaces. Indentation imposes a multiaxial stress state on a specimen—for the most part compressive, but the highly localized pressure gradients manifest themselves as shear stresses, of the order of average indentation pressure p_{ave}. It is clear from the optical micrographs (Fig. 7, 8) that inelasticity in the CS materials under indentation proceeds (at lower loads) via shear sliding at the large interfaces between particles.

In addition, photos suggest a significant friction component to the deformation. This can be demonstrated in the top three CS panels in Fig. 7. Under 50 and 100 N loading, interfacial sliding has occurred, but in contrast to APS and HVOF this is not directly under the contact tip, but rather at a significant distance beneath the surface. It is hypothesized that this is due to the high normal pressure near the tip that would increase the shear stress necessary to slide interfaces. (Note that HVOF and APS display similar characteristics in that inelasticity is observed at a short distance beneath the indenter tip. In the case of HVOF, very little interfacial sliding occurs, and inelasticity is presumably dominated by dislocation motion. This would presumably occur at the highest shear stress value, which occurs beneath the tip, at a distance of approximately $0.7a$ (Ref 29). In APS, inelasticity occurs in part via densification, and would thus occur in regions of highest pressure.) The CS assertion is sensible in the context of interfacial sliding; if cracks are a few nm thick (i.e., undetectable under SEM) and particles are of the order 10-50 microns in size, then small compressive strains (0.01%) in the particles would correspond to compressive deformation of 1-3 nm, giving significant gap closure/asperity contact. In APS/HVOF, interfaces are typically bonded, and pores have a lower aspect ratio (more rounded), so the effect of normal stress would not be as significant, as it would not lead to significant pore closure.

At higher loads, heterogeneous inelasticity of CS occurs (Fig. 5, 7). This can be explained via simplified fracture

mechanics arguments. Neglecting higher order terms and geometric constants, the criterion for fast fracture is that applied stress intensity factor K_{II} reaches material fracture toughness $K_{II\text{-}C}$. K_{II} is given by the formula

$$K_{II} = \sigma^{\infty}\sqrt{\pi a}$$

where σ^{∞} is the applied far field stress and a is the crack length. $K_{II\text{-}C}$ of CS Ni5Al is not known, but if perfect metallurgical bonding is assumed, then regions around the splats should exhibit values approaching 30 MPa $\sqrt{m}$. This value is perhaps an overestimation, as CS particles are severely work-hardened during impact, and the intermetallics could be expected to have lower toughness. Assuming crack lengths of the order of particle diameter (45 μm) then the far field stress required for fast fracture (not interfacial sliding) is of the order 1-2 GPa. This value is an approximation and is also dependent upon crack orientation, splat ductility, etc. Stresses of this magnitude are approached in the indentations of 300 N or greater in these experiments, and fracture is clearly observed in nearly all of these cases (Fig. 5, 7), leading to the asymmetry in the inelastic zone. Such behavior is not observed in APS and HVOF because such available defects do not exist. In the case of the multiple indents, the quasi-brittle nature of the CS materials is again shown, and fracture clearly favors the interfaces between particles.

The assertions in the preceding paragraph are supported by the impact tests (Fig. 9, 10) that show an increased data spread in the CS materials with increased impact load. APS and HVOF do not exhibit such an effect, and display no brittle events as the tests progress. Note that as these were dynamic tests, the effective 'contact' dimensions could be significantly larger than indicated by the tip displacement, due to the propagation of elastic waves. However, the exact magnitude of wave dissipation cannot be calculated from these experiments.

One important implication of this work is the potential damage under contact conditions; under medium contact loads (100-400 MPa), surface examination would not reveal the extent of subsurface cracking, delamination, etc., and perhaps cause overestimation of tribological performance. It would be interesting to see how this behavior changes for more (e.g., Al) or less (cermet) ductile materials.

5. Summary and Conclusions

In this study, modified indentation techniques were introduced to explore the inelastic behavior of metallic (Ni-5%Al) CS coatings over different size scales. This material exhibits quasi-brittle behavior, similar to other CS materials in as-sprayed condition. Inelasticity is dominated by the interfaces, to the extent that the material exhibits heterogeneities in mechanical behavior on a scale far above the several-splat length.

The following characteristics of inelasticity were observed for this material:

(1) In all experiments on CS, a spatially heterogeneous material response was exhibited on size scales of several hundred microns, with homogeneous response below this scale. This is in stark contrast to most sprayed materials that show homogeneous response above the several-splat size scale.

(2) Damage shows that cracking in CS materials does not occur where predicted from contact mechanics theory, and indicates that such behavior may be pressure-dependent.

(3) Under cyclic (fatigue) contact loading, CS materials are more brittle than APS and HVOF.

(4) In CS, results suggest incomplete bonding between particles, with crack length of the order of particle size. This assertion was supported by simple fracture mechanics arguments. In addition, under indentation loading it was asserted that interfacial toughness could be dependent upon applied normal pressure.

Acknowledgments

WBC, YW, and SS were supported by NSF GOALI-FRG 0605704. AG was supported by NSF CAREER CMS 0449268. The authors are grateful to H. Herman for helpful discussions. CS coatings were supplied by R.A. Neiser of Sandia National Laboratories.

References

1. A.P. Alkhimov, V.F. Kosarev, and A.N. Papyrin, A Method of Cold Gas-dynamic Spraying, *Sov. Phys. Dokl.*, 1990, **35**, p 1047-1049
2. R.C. Dykhuizen and M.F. Smith, Gas Dynamic Principles of Cold Spray, *J. Therm. Spray Technol.*, 1998, **7**, p 205-212
3. R.C. Dykhuizen, M.F. Smith, D.L. Gilmore, R.A. Neiser, X.S. Jiang, and S. Sampath, Impact of High Velocity Cold-spray Particles, *J. Therm. Spray Technol.*, 1999, **8**, p 559-564
4. D.L. Gilmore, R.C. Dykhuizen, R.A. Neiser, T.J. Roemer, and M.F. Smith, Particle Velocity and Deposition Efficiency in the Cold Spray Process, *J. Therm. Spray Technol.*, 1999, **8**, p 576-582
5. T.H. Van Steenkiste, J.R. Smith, and R.E. Teets, Aluminum Coatings Via Kinetic Spray with Relatively Large Powder Particles, *Surf. Coat. Technol.*, 2002, **154**, p 237-252
6. C.J. Li and W.Y. Li, Deposition Characteristics of Titanium Coating in Cold Spraying, *Surf. Coat. Technol.*, 2003, **167**, p 278-283
7. A.P. Alkhimov, V.F. Kosarev, and A.N. Papyrin, Gas-dynamic Spraying. An Experimental Study of the Spraying Process, *J. Appl. Mech. Techn. Phys.*, 1998, **39**, p 318
8. C.J. Li, L.W.Y. Li, and H. Fukanuma, Ed., *International Thermal Spray Conference*, 2004, Osaka, Japan
9. H.J. Kim, C.H. Lee, and S.Y. Hwang, Fabrication of WC-Co Coatings by Cold Spray Deposition, *Surf. Coat. Technol.*, 2005, **191**, p 335-340
10. H.Y. Lee, Y.H. Yu, Y.C. Lee, Y.P. Hong, and K.H. Ko, Alloying of Cold Sprayed Al-Ni Composite Coatings by Post-annealing, *Appl. Surf. Sci.*, 2004, **227**, p 3496-3502
11. R.S. Lima, J. Karthikeyan, C.M. Kay, J. Lindemann, and C.C. Berndt, Microstructural Characteristics of Cold-sprayed Nanostructured WC-Co Coatings, *Thin Solid Films*, 2002, **416**(1), p 129-135
12. H. Assadi, F. Gartner, T. Stoltenhoff, and H. Kreye, Bonding Mechanism in Cold Gas Spraying, *Acta Mater.*, 2003, **51**, p 4379-4394

13. S. Sampath, X.Y. Jiang, J. Matejicek, L. Prchlik, A. Kulkarni, and A. Vaidya, Role of Thermal Spray Processing Method on the Microstructure, Residual Stress and Properties of Coatings: An Integrated study for Ni-5wt.%Al Bond Coats, *Mater. Sci. Eng. A-Struct.*, 2004, **364**, p 216-231
14. W.B. Choi, L. Li, V. Luzin, R.A. Neiser, T. Gnaupel-Herold, H.J. Prask, S. Sampath, and A. Gouldstone, Integrated Characterization of Cold Spray Aluminum Coatings, *Acta Mater.*, 2007, **55**, p 857-866
15. A.C. Hall, D.J. Cook, R.A. Neiser, and T.J. Roemer, The Effect of a Simple Annealing Heat Treatment on the Mechanical Properties of Cold-sprayed Aluminum, *Proceedings of ITSC 2005*, Basel, Switzerland, 2005
16. A. Pajares, L. Wei, B.R. Lawn, and C.C. Berndt, Contact Damage in Alumina-based Plasma Sprayed Coatings, *J. Am. Ceram. Soc.*, 1996, **79**(7), p 1907-1914
17. L. Prchlik, J. Pisacka, and S. Sampath, Deformation and Strain Distribution in Plasma Sprayed Nickel-aluminum Coating Loaded by a Spherical Indenter, *Mater. Sci. Eng. A-Struct.*, 2003, **360**, p 264-274
18. F. Gärtner, T. Stoltenhoff, T. Schmidt, and H. Kreye, The Cold Spray Process and its Potential for Industrial Applications, *J. Therm. Spray Technol.*, 2006, **15**, p 223-232
19. F. Guiberteau, N.P. Padture, H. Cai, and B.R. Lawn, Indentation Fatigue. A Simple Cyclic Hertzian Test for Measuring Damage Accumulation in Polycrystalline Ceramics, *Philos. Mag. A*, 1993, **68**, p 1003-1016
20. F. Guiberteau, N.P. Padture, and B.R. Lawn, Effect of Grain Size on Hertzian Contact Damage in Alumina, *J. Am. Ceram. Soc.*, 1994, **77**, p 1825-1831
21. ABAQUS Finite Element Package 6.5. Hibbit, Karlson, Sorenson Inc. Pawtucket, RI, 2005
22. B.D. Beake and J.F. Smith, Evaluating the Fracture Properties and Fatigue Wear of Tetrahedral Amorphous Carbon Films on Silicon by Nano-impact Testing, *Surf. Coat. Technol.*, 2004, **188**, p 594-598
23. B.D. Beake, S.R. Goodes, J.F. Smith, and F. Gao, Nanoscale Repetitive Impact Testing of Polymer Films, *J. Mater. Res.*, 2004, **19**, p 237-247
24. X. Guo, G. Zhang, W.Y. Li, L. Dembinski, Y. Gao, H.L. Liao, and C. Coddet, Microstructure, Microhardness and Dry Friction Behavior of Cold-sprayed Tin Bronze Coatings, *Appl. Surf. Sci.*, 2007, **254**(5), p 1482-1482
25. K. Balani, A. Agarwal, S. Seal, and J. Karthikeyan, Transmission Electron Microscopy of Cold Sprayed 1100 Aluminum Coating, *Scripta Mater.*, 2005, **53**, p 845-850
26. R.C. McCune, A.N. Papyrin, J.N. Hall, L.W. Riggs, P.H. Zajchowski, C.C. Berndt, and S. Sampath, Ed., *Thermal Spray Science & Technology 1995*, Houston, TX, ASM International, Materials Park, OH, 1995
27. P. Fauchais, M. Fukumoto, A. Vardelle, and M. Vardelle, Knowledge Concerning Splat Formation, an Invited Review, *J. Therm. Spray Technol.*, 2004, **13**, p 337-360
28. T.S. Price, P.H. Shipway, D.G. McCartney, E. Calla, and D. Zhang, A Method for Characterizing the Degree of Inter-particle Bond Formation in Cold Sprayed Coatings, *J. Therm. Spray Technol.*, 2007, **16**, p 566-570
29. K.L. Johnson, *Contact Mechanics*, Chap. 4, Cambridge University Press, Cambridge, UK, 1985